Four-Wave Mixing Dipole Soliton in Laser-Induced Atomic Gratings

Yanpeng Zhang,[1,*] Zhiguo Wang,[1] Zhiqiang Nie,[1] Changbiao Li,[1] Haixia Chen,[1] Keqing Lu,[1] and Min Xiao[2,3,†]

[1]*Key Laboratory for Physical Electronics and Devices of the Ministry of Education & Shaanxi Key Lab of Information
Photonic Technique, Xi'an Jiaotong University, Xi'an 710049, China*
[2]*Department of Physics, University of Arkansas, Fayetteville, Arkansas 72701, USA*
[3]*National Laboratory of Solid State Microstructures and Department of Physics, Nanjing University, Nanjing 210093, China*
(Received 5 September 2010; published 4 March 2011)

We demonstrate a novel type of stable multicomponent vector solitons consisting of two perpendicular
four-wave mixing (FWM) dipole components induced by electromagnetically induced gratings. We
analyze the formation and steering of the steady dipole solitons and their dynamical (energy transfer)
effects. The dipole-mode solitons of two FWM processes have horizontal and vertical orientations,
respectively. Omnidirectional Bragg reflections are also investigated.

Spatial solitons can form when the diffraction of a laser beam is compensated by the self-focusing effect in a Kerr nonlinear medium [1,2]. If a phase mask is used to introduce a π phase delay for half of the soliton beam, the soliton can split into two parts with opposite phases between them, called dipole-mode vector soliton with a Hermite-Gaussian mode structure [3]. In an optically induced two-dimensional photonic lattice, dipole-mode solitons can be created with either opposite phases or same phase between the two parts [4]. Vector solitons with one nodeless fundamental component and another dipole-mode component can couple to each other and be trapped jointly in the photonic lattices [3,5]. A radially symmetric vortex soliton can decay into a radially asymmetric dipole-mode soliton with a nonzero angular momentum, which can survive for a very long propagation distance [3]. In the past few years, studying formation and properties of such novel spatial solitons has become an active field of research [1–12]. Much more recently, the spatial gap solitons in atomic medium were experimentally demonstrated [13].

In this Letter, we show that such charged dipole-mode solitons can also be created in the four-wave mixing (FWM) beams generated inside a multilevel atomic medium, in which the self-Kerr and cross-Kerr nonlinearities are greatly enhanced by laser-induced atomic coherences [14]. The key to observe such novel dipole-mode solitons is to create a high enough index contrast (via Kerr nonlinearity n_2I) in the atomic medium by laser-induced index gratings. Two-component dipole-mode solitons are generated in two coexisting FWM signal beams in a three-level atomic system. The easy controls of experimental parameters in the multilevel atoms make the current system ideal to investigate the formations of multicomponent spatial solitons and their nonlinear dynamics [6–8].

Laser beams are spatially aligned in the configuration as shown in Fig. 1(a). Energy levels $|0\rangle$ ($3S_{1/2}$), $|1\rangle$ ($3P_{1/2}$) and $|2\rangle$ ($4D_{3/2}$) in sodium atoms form a cascade three-level system [Fig. 1(b)]. Two laser fields E_1 and E_1' (with Rabi

frequencies G_1 and G_1', and frequency ω_1) connecting the transition $|0\rangle$ to $|1\rangle$, with an angle $\theta_1 \approx 0.3°$ between them, propagate in the opposite direction of a weak probe field E_3 (with Rabi frequency G_3 and frequency ω_1). The three beams are from the same near-transform-limited dye laser (10 Hz repetition rate, 5 ns pulse-width and 0.04 cm^{-1} linewidth). They generate an efficient one-photon resonant FWM signal E_{F1} satisfying the phase-matching condition of $\mathbf{k}_{F1} = \mathbf{k}_3 + \mathbf{k}_1 - \mathbf{k}_1'$, which propagates nearly opposite to the field E_1', and is sampled by a CCD camera. Two additional coupling fields E_2 and E_2' (with Rabi frequencies G_2 and G_2', and an angle $\theta_2 \approx 0.3°$ between them) are used to drive the transition $|1\rangle$ to $|2\rangle$, which are from another
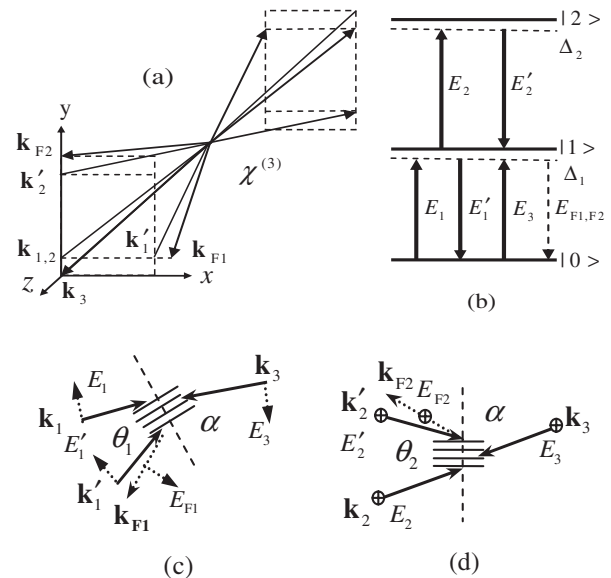
FIG. 1.   (a) Spatial beam geometry used in the experiment. (b) Two FWM processes E_{F1} and E_{F2}, with five beams E_1, E_1', E_2, E_2', and E_3 on, in a cascade three-level atomic system. E_{F1} (TM polarization) in (c) and E_{F2} (TE polarization) in (d) are mainly steered by the horizontally and vertically aligned EIG1 and EIG2, respectively.

similar dye laser with frequency ω_2. E_2, E_2', and E_3 generate a two-photon resonant FWM signal E_{F2} with $\mathbf{k}_{F2} = \mathbf{k}_3 + \mathbf{k}_2 - \mathbf{k}_2'$, propagating nearly opposite to the field E_2' [Fig. 1(a)] [15]. The coherence lengths for E_{F1} and E_{F2} are $L_{F1}^c = 2c\pi\omega_1/(n_1\omega_1|\omega_1 - \omega_1|\theta_1^2) \rightarrow \infty$ and $L_{F2}^c = 2c\pi\omega_1/(n_1\omega_2|\omega_2 - \omega_1|\theta_2^2) \approx 0.6$ m, respectively, where n_1 is the linear refractive index. All incident beams are P polarized.

Two-component dipole solitons are formed by the balanced interactions between spatial diffractions and cross-Kerr nonlinearities of the fields $E_{1,2}$ and $E_{1,2}'$. To generate dipole-mode solitons, the sodium atomic density needs to reach 2.9×10^{13} cm^{-3} ($T = 250°C$), which can produce the needed variation in the nonlinear index of $\Delta n = 1.94 \times 10^{-4}$ at high enough laser intensities.

Let us consider two electromagnetically induced gratings (EIG) in the atomic medium [16]. EIG can form when the weak probe beam E_3, coupled to one atomic transition, interacts with two strong noncollinear beams [either beams E_1 and E_1' in Fig. 1(c), or E_2 and E_2' in Fig. 1(d)], that is coupled to the same or different atomic transition in an atomic medium. The beams E_1 and E_1' (or beams E_2 and E_2') induce their own grating EIG1 (or EIG2). Such periodic refractive-index changes create

two photonic band gaps, which prohibit the probe propagation and give rise to the highly efficient omnidirectional reflections [17]. Thus, the FWM signals (E_{F1} and E_{F2}) are the results of the electromagnetically induced diffraction (EID) of the probe beam E_3 by the induced EIG1 and EIG2, respectively. The fringe spacings of EIG1 and EIG2 are determined by $a_i = \lambda_i/\theta_i$ ($i = 1, 2$). The dipole-like patterns of E_{F1} and E_{F2} are created by the horizontally and vertically aligned EIG1 and EIG2, respectively. One of the advantages of such spatial solitons is that the wave guiding effect is induced by focusing due to the cross-Kerr nonlinearity of the FWM beam, not self-focusing which normally suffers catastrophic absorption [12].

A radially asymmetric dipole-mode vector soliton includes one nodeless component (the probe beam E_3) and two dipolelike components with spatial structures of Hermite-Gaussian modes (HG$_{10}$ for E_{F1} and HG$_{01}$ for E_{F2}). We mainly study two coupled FWM beams E_{F1} and E_{F2} (with the same frequency), which have perpendicularly oriented dipole components, propagating along z direction and diffusing along one transverse direction. We assume $E_{F1} = A_{F1}(\zeta)\exp(ik_{F1}z)$, $E_{F2} = A_{F2}(\zeta)\exp(ik_{F2}z)$, and $E_{tot} = E_{F1} + E_{F2}$. These two coupled FWM fields satisfy the evolution equations in the Kerr medium as

$$\frac{\partial A_{F1}}{\partial z} - \frac{i\nabla_\perp^2 A_{F1}}{2k_{F1}} = \frac{ik_{F1}}{n_1}(n_2^{S1}|A_{F1}|^2 + 2n_2^{X1}|A_1|^2 + 2n_2^{X2}|A_1'|^2 + 2n_2^{X3}|A_2'|^2)A_{F1} + \eta_1 A_1(A_1')^*A_{F2}, \tag{1a}$$

$$\frac{\partial A_{F2}}{\partial z} - \frac{i\nabla_\perp^2 A_{F2}}{2k_{F2}} = \frac{ik_{F2}}{n_1}(n_2^{S2}|A_{F2}|^2 + 2n_2^{X4}|A_2|^2 + 2n_2^{X5}|A_2'|^2 + 2n_2^{X6}|A_1'|^2)A_{F2} + \eta_2 A_2(A_2')^*A_{F1}. \tag{1b}$$

Two-component dipole-mode solitons are natural results from such energy-dependent nonlinear propagation equations. $n_2^{S1,S2}$ are self-Kerr nonlinear coefficients of E_{F1} and E_{F2}, and n_2^{X1-X6} are cross-Kerr nonlinear coefficients of $E_{1,2}$ and $E_{1,2}'$ to E_{F1} and E_{F2}, respectively. The Kerr nonlinear coefficient is defined as $n_2 = \text{Re}\chi^{(3)}/(\varepsilon_0 c n_1)$. The dressed third-order nonlinear susceptibility is $\chi^{(3)} = D\rho_{10}^{(3)}$, where $D = N\mu_{10}^4/(\hbar^3\varepsilon_0 G_{F1,F2}G_i^2)$ ($G_{F1,F2}$ are Rabi frequencies of $E_{F1,F2}$, respectively), and spatially modulated density-matrix element $\rho_{10}^{(3)} \propto 1/\prod_{i=1}^3[a_i + G_j^2\cos^2(k_2\zeta)]$ ($\zeta = x, y$). N is the atomic density and μ_{ij} is the dipole-matrix element between $|i>$ and $|j>$. By solving the density-matrix equations of the cascade three-level atomic system, detail expressions of all the self- and cross-Kerr nonlinear indices can be obtained. $\eta_1 = \xi\mu_{10}^5 F_a$ and $\eta_2 = \xi\mu_{21}^5 F_b$ with $\xi = i4\pi\omega_1 N/ch^4$, where F_a and F_b relate to the Rabi frequencies of the involved fields, the frequency detuning Δ_1 (Δ_2) for $E_{1,3,F1,F2}$ and E_1' (E_2 and E_2'), and the relaxation rates of the system [14].

The resulting superposition of the two perpendicular dipole-soliton components, E_{F1} and E_{F2}, is a generalization

from a two-component dipole-mode soliton (E_3, E_F) to a three-component one (E_3, E_{F1}, E_{F2}). The total intensity ($I = |E_3|^2 + |E_{F1}|^2 + |E_{F2}|^2$) is quasistable in propagation after a long enough propagation distance (or high enough atomic density). The three components of the vector soliton carry topological charges 0, $+1$, -1, respectively, and the total angular momentum is zero ($m_{F1} + m_{F2} + m_3 = 0$), which makes the solution stable [7], where $m_{3,F1,F2}$ are topological charges of $E_{3,F1,F2}$.

The in-phase dipole modes of E_{F1} and E_{F2} are created (or split) by the horizontally- and vertically-aligned EIG1 and EIG2, respectively. Thus, the two-component dipole-mode soliton solutions of E_{F1} and E_{F2} can be written as $E_{F1} = u_1\text{sech}[u_1(k_{F1}n_2^{S1}/n_0)^{1/2}(r - r_1)] \times \cos(M\varphi/2)\exp(im_{F1}\varphi + i\phi_1)\exp(ik_{F1}z)$ and $E_{F2} = u_2\text{sech}[u_2(k_{F2}n_2^{S2}/n_0)^{1/2}(r - r_2)]\cos(M\varphi/2)\exp(im_{F2}\varphi + i\phi_2)\exp(ik_{F2}z)$, where $u_{1,2}$ are soliton amplitudes; $r_{1,2}$ are initial peak positions; M is the number of intensity peaks; $\phi_{1,2}$ are nonlinear phase shifts ($\phi_{1,2} = 2k_{1,2}n_2 I_{2,1}e^{-r^2/2}z/n_1$). Such solutions possess the dipole-soliton characteristics, and two humps form the two poles of the dipole soliton, which are trapped jointly in the neighbor photonic fringes.

The generated FWM (E_{F2}) beam can be significantly influenced by the dressing beams G_1', G_1, or G_1' & G_1 in the cascade three-level system (Fig. 2). We present the vertical dipole-mode solitons of E_{F2} with different dressing configurations. The E_{F2} beam splits into two coherent spots (i.e., dipole pattern, as shown in Fig. 2) due to the modulated transverse nonlinear phase shift ϕ_2 induced by the vertically-aligned EIG2. At low nonlinear dispersion $|n_2|$, E_{F2} beam only experiences the linear diffraction. With maximum $|n_2|$ at $|\Delta_1| = 16.5$ GHz [Fig. 2(b)], vertically oriented dipole soliton is generated due to the balanced interaction between the spatial diffraction and the cross-Kerr nonlinearity. At resonance or large frequency detunings, the dipole-mode soliton of E_{F2} decays into a nodeless fundamental one. Under the case of enhanced FWM due to dressing (satisfying $\Delta_1 + \Delta_2 = |G_1 + G_1'|^2/\Delta_2$ [15]) in Fig. 2(a), E_{F2} with both G_1' and G_1 dressing is stronger than with G_1' or G_1 dressing separately, or without dressing fields. For stronger G_1', the dressing effect of G_1' is larger than that of G_1. In the enhancement case with $\Delta_1 = 16.5$ GHz, the nonlinear refractive index is $n_2 = -9 \times 10^{-7}$ cm^2/W for E_{F2}, which is much larger than $n_2 = -2 \times 10^{-8}$ cm^2/W in the suppressed case with $\Delta_1 = 4.5$ GHz (satisfying $\Delta_1 + \Delta_2 \approx 0$). The cross-Kerr nonlinearity in the enhancement case can well compensate the diffraction in the propagation, while it is too weak to balance the diffraction without the enhancement.

When five laser beams are turned on at the same time in the cascade three-level system, the probe beam forms a fundamental nodeless soliton and propagates with a stable shape for different atomic densities (equivalent to different propagation distances), as shown in Fig. 3(a). The effective propagation distance of such soliton is 10.8 times longer than the diffraction length ($L_D = k_1 d^2 \approx 0.96$ cm with a beam diameter of $d \approx 30$ μm) [12]. However, the beam shapes of E_{F1} and E_{F2} become quite different at different propagation distances showing rich dynamical behaviors. The probe, E_{F1} and E_{F2} beams have the same wavelength. E_{F1} beam has the dipole component with the horizontal orientation ($m_{F1} = -1$) while E_{F2} beam gives the vertical dipole component ($m_{F2} = +1$), which are induced by the horizontally and vertically aligned EIG1 and EIG2, respectively. During the propagation of E_{F1} (or E_{F2}) beam, energy flows back and forth between the two spots, so the dipole solitons of E_{F1} and E_{F2} survive with a strong oscillation (or breathing) in propagation. The superposition of these modes shows intriguing dynamics, associated with a rotational instability in $E_{F1} + E_{F2}$ [7]. The fundamental probe soliton is stable, which has a stronger contribution to the total superposition mode. Moreover, when the propagation distance increases gradually, one can see energy transfers among the probe, E_{F1} and E_{F2} beams, as shown in the right panel of Fig. 3(a). The total intensity of the probe, E_{F1} and E_{F2} reaches a steady state after a long interaction distance (i.e., no energy exchange afterward).

For certain frequency detunings, the energy of the dipole soliton can be trapped in one part or another. With Δ_1

FIG. 2 (color online). Images at different Δ_1 (i)–(iv) and beam profiles at $\Delta_1 = 16.5$ GHz (a) of dipole-soliton E_{F2} in the cascade three-level system with $G_2' = G_2 = 20$ GHz, $G_1' = 55$ GHz and $G_1 = 45$ GHz ((i) and squares), $G_1' = 55$ GHz and $G_1 = 0$ [(ii) and circles], $G_1' = 0$ and $G_1 = 45$ GHz [(iii) and triangles], and without dressing fields [(iv) and diamonds]. (b) Nonlinear refractive index n_2 of E_{F2} with G_1' and G_1 dressings [15].
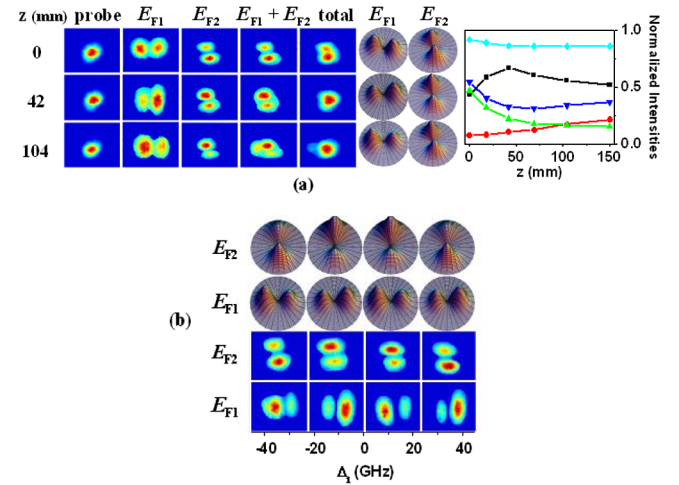
FIG. 3 (color online). (a) Experimental (left) and numerical (middle) results of three-component dipole solitons of the probe, E_{F1} and E_{F2} beams with $z = 0, 42, 104$ in the cascade three-level system at $\Delta_1 = -15$ GHz, $\Delta_2 = -4.5$ GHz. Intensity changes (right panel) of the dipole-soliton components during propagation for the probe (squares), E_{F1} (circles), E_{F2} (triangles), $E_{F1} + E_{F2}$ (reverse triangles), and total (diamonds) fields. (b) Breathing effects of E_{F1} (lower) and E_{F2} (upper) versus Δ_1. The top panel gives the numerical results.
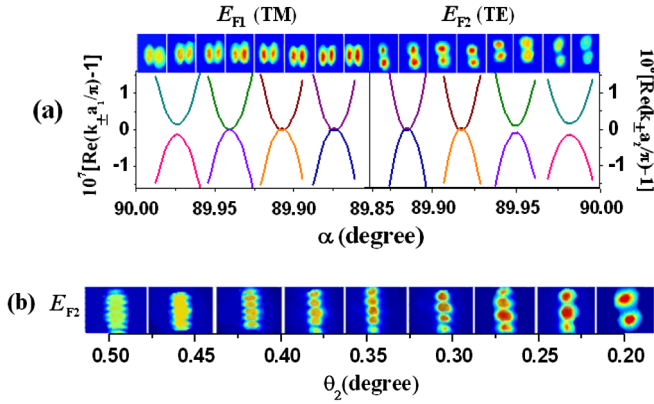
FIG. 4 (color online). Omnidirectional Bragg reflections of E_{F1} and E_{F2} beams versus α (a), and E_{F2} beam versus θ_2 (b), the solid curves are calculated results of Bloch wave-vectors $\mathrm{Re}(k_\pm)$. The parameters are $\Delta_1 = -15$ GHz, $\Delta_2 = -4.5$ GHz, $G_1' = G_1 = G_2' = G_2 = 20$ GHz, and $G_3 = 0.5$ GHz.

changes from -26 GHz to -10 GHz in the self-focusing regime, energy flows from the left spot of E_{F1} (or upper spot of E_{F2}) to the right (or lower) spot. Symmetric behaviors appear in the positive frequency detuning (self-defocusing) side [Fig. 3(b)]. Since the phase ϕ in the current dipole solution has values $0 < \phi < \pi$ (the out-of-phase repelling dipole soliton is more stable than the in-phase attracting one) [4,5], the energy exchange occurs periodically.

The spatially modulated total linear and nonlinear refractive index is given by $n(\zeta) = n_0 + \delta n_1 \cos(2k_2\zeta) + \delta n_2 \cos(4k_2\zeta)$, where n_0 is the spatially uniform refractive index; δn_1 and δn_2 are the coefficients for spatially varying terms for the modulated index. The width of the band gap is given by $\Delta_{\mathrm{gap}} = 2\omega_0(\delta n_1 + \delta n_2)/\pi n_0$, where ω_0 is the center frequency of the forbidden band. Moreover, by coupled mode techniques with Bloch's theorem, we can get $k_\pm = k_i \pm (\{k_p^2[1 + \chi_1 + (\chi_2^2 - \chi_3^2)\chi_2'] - k_i^2\}^2 - k_p^4[\chi_2\chi_3\chi_2' + (\chi_2^2 + 2\chi_2\chi_3)\chi_3']^2)^{1/2}/2k_i$ (with $k_p = k_3\cos\alpha$), and obtain the dispersion curves of $\mathrm{Re}(k_\pm a_i/\pi - 1)$ versus Δ_1 ($i = 1, 2$ are for E_{F1} and E_{F2}, respectively), as shown in Fig. 4(a). Here, $k_\pm$ are the Bloch wave-vectors near the Brillouin zone edge, and χ_m & χ_m' ($m = 1, 2, 3$) are the susceptibility components. Also, with increasing incident angle α of the probe beam E_3 from $89.85°$ to $90°$, as shown in Figs. 1(c) and 1(d), there exist a series of forbidden bands (the region with $\mathrm{Re}(k_\pm a_i/\pi - 1) \approx 0$ in Fig. 4(a), with right side for the TE-polarized E_{F2} cases and left side for the TM-polarized E_{F1} cases, respectively) for such induced periodic medium, which result from the strong omnidirectional Bragg reflections [17]. It is obvious that the dipole-mode E_{F1} and E_{F2} soliton beams become weaker (as the stop bands start to disappear from $89.95°$ to $90°$ for the incident angle). When the band gap completely disappears at $89.975°$ (with no zero values for the real dispersion, as shown in the far right and far left

dispersion curves), the residual intensity comes from the FWM signal without the Bragg reflection. In Fig. 4(b), when the angle θ_2 between the beams E_2 and E_2' decreases, the number of spots for the E_{F2} beam changes from eight into two (dipole-mode). The energy has been transferred from those eight spots (at $\theta_2 = 0.5°$) to the dipole-mode spots (at $\theta_2 = 0.2°$). Such dipole soliton is trapped jointly in the neighboring photonic fringes. Since $a_2 = \lambda_2/\theta_2$, the fringe spacing of EIG2 will become larger versus decreasing θ_2.

In conclusion, we have experimentally demonstrated controllable dipole-mode solitons for generated FWM beams in the three-level cascade atomic system. This study exploits new ways in controlling the diffraction and propagation of optical beams, and in designing new devices for spatial optical switching and logic gating in optical communication and all-optical signal processing.

*ypzhang@mail.xjtu.edu.cn
†mxiao@uark.edu

[1] Y. S. Kivshar and G. P. Agrawal, *Optical solitons: From Fibers to Photonic Crystals* (Academic, San Diego, 2003).
[2] G. A. Swartzlander, Jr. and C. T. Law, Phys. Rev. Lett. **69**, 2503 (1992).
[3] W. Krolikowski, E. A. Ostrovskaya, and C. Weilnau *et al.*, Phys. Rev. Lett. **85**, 1424 (2000).
[4] J. K. Yang, I. Makasyuk, and A. Bezryadina *et al.*, Opt. Lett. **29**, 1662 (2004).
[5] Z. G. Chen, A. Bezryadina, and I. Makasyuk *et al.*, Opt. Lett. **29**, 1656 (2004).
[6] A. S. Desyatnikov and Y. S. Kivshar, Phys. Rev. Lett. **87**, 033901 (2001).
[7] A. S. Desyatnikov, Y. S. Kivshar, and K. Motzek *et al.*, Opt. Lett. **27**, 634 (2002).
[8] D. Neshev, G. McCarthy, and W. Krolikowski *et al.*, Opt. Lett. **26**, 1185 (2001).
[9] L. G. Tang, C. B. Lou, and X. S. Wang *et al.*, Opt. Lett. **32**, 3011 (2007).
[10] C. Becker, S. Stellmer, and P. Soltan-Panahi *et al.*, Nature Phys. **4**, 496 (2008).
[11] V. Boyer, A. M. Marino, R. C. Pooser, and P. D. Lett, Science **321**, 544 (2008).
[12] D. Bortman-Arbiv, A. D. Wilson-Gordon, and H. Friedmann, Phys. Rev. A **58**, R3403 (1998).
[13] Y. P. Zhang, Z. G. Wang, and H. B. Zheng *et al.*, Phys. Rev. A **82**, 053837 (2010).
[14] H. Wang, D. Goorskey, and M. Xiao, Phys. Rev. Lett. **87**, 073601 (2001).
[15] Y. P. Zhang, C. C. Zuo, and H. B. Zheng *et al.*, Phys. Rev. A **80**, 055804 (2009).
[16] H. Y. Ling, Y. Q. Li, and M. Xiao, Phys. Rev. A **57**, 1338 (1998).
[17] Y. Fink, J. N. Winn, and S. Fan *et al.*, Science **282**, 1679 (1998).